

Generating synthetic Landsat images based on all available Landsat data: Predicting Landsat surface reflectance at any given time



Zhe Zhu ^{a,*}, Curtis E. Woodcock ^a, Christopher Holden ^a, Zhiqiang Yang ^b

^a Center for Remote Sensing, Department of Earth and Environment, Boston University, 685 Commonwealth Avenue, Boston, MA 02215, United States

^b Department of Forest Ecosystems and Society, Oregon State University, 321 Richardson Hall, Corvallis, OR 97331, United States

ARTICLE INFO

Article history:

Received 5 October 2014

Received in revised form 8 January 2015

Accepted 7 February 2015

Available online xxxx

Keywords:

Synthetic
Landsat
Surface reflectance
Time series model
Predict

ABSTRACT

A new algorithm for generating synthetic Landsat images is developed based on all available Landsat data. This algorithm is capable of predicting Landsat surface reflectance for any desired date. It first excludes cloud, cloud shadow, and snow observations, and then uses the remaining clear observations to estimate time series models for each Landsat pixel. Three time series models (a simple model, advanced model, and full model) are used for estimating surface reflectance for each pixel, and the selection of a time series model is dependent on the number of clear observations available: the more clear observations, the more complex the model will be that is used. For each time series model there are three components (seasonality, trend, and breaks), that are used for modeling intra-annual and inter-annual differences and abrupt surface change. Abrupt surface changes are detected by differencing predicted and observed Landsat observations, and if the difference is larger than twice the Root Mean Square Error (RMSE) for six consecutive observations, it will be detected as a “break” in the time series model. The RMSE values are temporally adjusted to provide better threshold range. For each “synthetic” image, a Quality Assessment (QA) Band is provided that contains information on how the time series model was estimated and used for generating the synthetic data. We have applied this approach to six Landsat scenes within the United States. We visually compared the synthetic images with real Landsat images for different kinds of environments and they are similar for all image pairs. We also quantitatively assessed the accuracy of the synthetic data by calculating the RMSE value for all clear Landsat observations. The RMSE values for the three visible bands are the lowest (approximately 0.01), and the Short-wave Infrared (SWIR) bands are slightly higher in magnitude (between 0.01 and 0.02). The Near Infrared (NIR) band has the highest RMSE values (between 0.02 and 0.03). The goal of this paper is to provide Landsat images that are free of cloud, cloud shadow, snow, and Scan Line Corrector (SLC)-off gaps that can be used to derive land cover and bio-physical products.

© 2015 Elsevier Inc. All rights reserved.

1. Introduction

The Landsat satellite series provides the longest record of earth observations (Williams, Goward, & Arvidson, 2006). Due to its relatively high spatial resolution, accurate radiometric calibration, and high geometric precision, it has been widely used in many aspects of remote sensing activities. In January 2008, U.S. Geological Survey (USGS) started to provide Landsat data at no cost via the Internet, which makes Landsat data even more popular (Woodcock et al., 2008; Wulder, Masek, Cohen, Loveland, & Woodcock, 2012). With the freely available Landsat data, it is now possible to reconstruct the history of the Earth's surface back to 1972 (Pflugmacher, Cohen, & Kennedy, 2012).

Despite all these advantages, Landsat data also have limitations and issues. The most significant limitation is its relatively low temporal frequency (16 day revisit capability). For each Landsat sensor, if every overpass is acquired, only 22 or 23 acquisitions per year per Path/Row

are collected (Ju & Roy, 2008). Moreover, due to the limited duty cycles, the lack of on-board data recording capabilities, and the constraints of international ground stations, the Landsat project does not acquire every acquisition globally (Arvidson, Goward, Gasch, & Williams, 2006). Additionally, the presence of cloud, cloud shadow, and snow further reduce the number of available clear Landsat observations (hereafter “clear” refers to observations that are free of cloud, cloud shadow, and snow). For example, the annual mean cloud cover for all

Table 1

The six optical Landsat TM/ETM+ spectral bands used for generating synthetic Landsat images.

TM bands (μm)	ETM+ bands (μm)
Band 1 (0.45–0.52)	Band 1 (0.45–0.515)
Band 2 (0.52–0.60)	Band 2 (0.525–0.605)
Band 3 (0.63–0.69)	Band 3 (0.63–0.69)
Band 4 (0.76–0.90)	Band 4 (0.75–0.90)
Band 5 (1.55–1.75)	Band 5 (1.55–1.75)
Band 7 (2.08–2.35)	Band 7 (2.09–2.35)

* Corresponding author. Tel.: +1 617 233 6031.
E-mail address: zhuzhe@bu.edu (Z. Zhu).

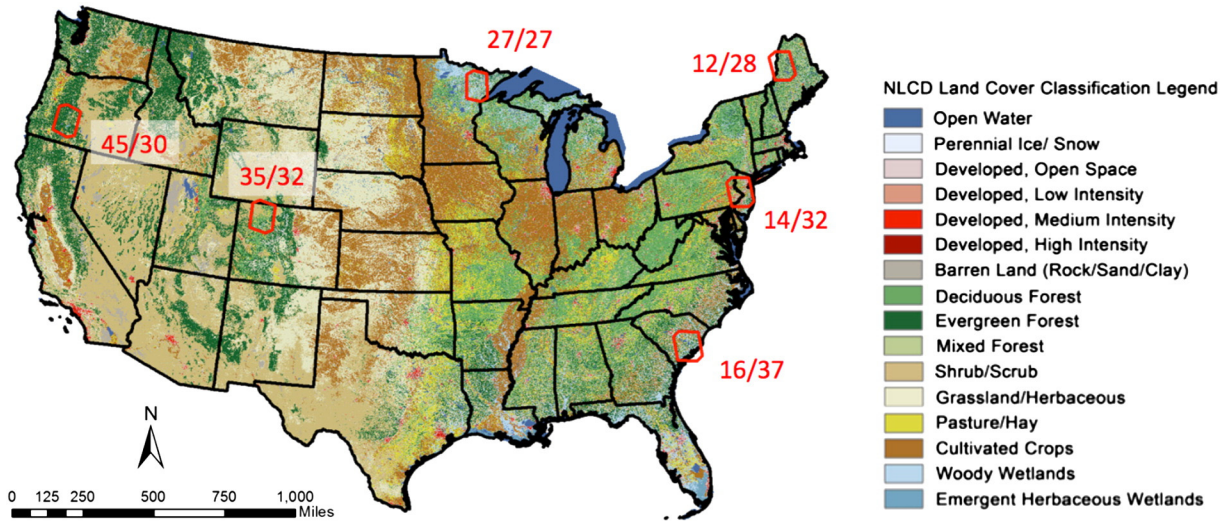


Fig. 1. Six study sites (red polygons are Landsat scenes by Path/Row), shown in the context of the 2006 National Land Cover Database (NLCD) cover map (Fry et al., 2011). (For interpretation of the references to color in this figure legend, the reader is referred to the web version of this article.)

Landsat Enhanced Thematic Mapper Plus (ETM+) images stored in the U.S. Landsat archive is approximately 35% (Ju & Roy, 2008). What is more, the failure of the ETM+ Scan Line Corrector (SLC) that occurred in May 2003 reduces the total usable data in each Landsat ETM+ image by 22% (Maxwell, Schmidt, & Storey, 2007). Therefore, it is very difficult to find entire Landsat images that are free of cloud, cloud shadow, snow, and without SLC-off artifacts for a specified time period.

Image compositing has been shown to be a powerful tool for generating clear satellite images. There are many compositing methods available (Cihlar, Manak, & D'lorio, 1994; Griffiths, van der Linden, Kuemmerle, & Hostert, 2013; Hansen et al., 2008; Holben, 1986; Luo, Trishchenko, & Khlopenkov, 2008; Roy et al., 2010; Stoms, Bueno, & Davis, 1997;

White et al., 2014), either based on single criteria (e.g. maximum NDVI, minimum red Band, or maximum brightness temperature), or multiple criteria to select the “best” observation with minimum cloud, cloud shadow, and snow contamination. However, most of the existing image compositing methodologies are designed for satellite data with high temporal frequency, such as Moderate Resolution Imaging Spectroradiometer (MODIS) and Advanced Very High Resolution Radiometer (AVHRR), and only a few studies are applied for satellite data with relatively low temporal frequency like Landsat data (Griffiths et al., 2013; Hansen et al., 2008; Hermosilla, Wulder, White, Coops, & Hobart, 2015; Roy et al., 2010; White et al., in press). Due to the lack of frequent observations, it may take a few months or even years to provide

Table 2
The acquisition date for the first and the last Landsat images (month/day/year) and total number of Landsat images used to generate synthetic Landsat image for each Path/Row.

Path/Row	27/27	12/28	45/30	35/32	14/32	16/37
First image	12/08/1982	05/18/1984	06/26/1984	04/17/1984	11/27/1982	04/12/1984
Last image	11/08/2012	09/28/2012	11/22/2012	05/27/2013	06/25/2013	07/25/2013
# of images	312	257	486	447	482	617

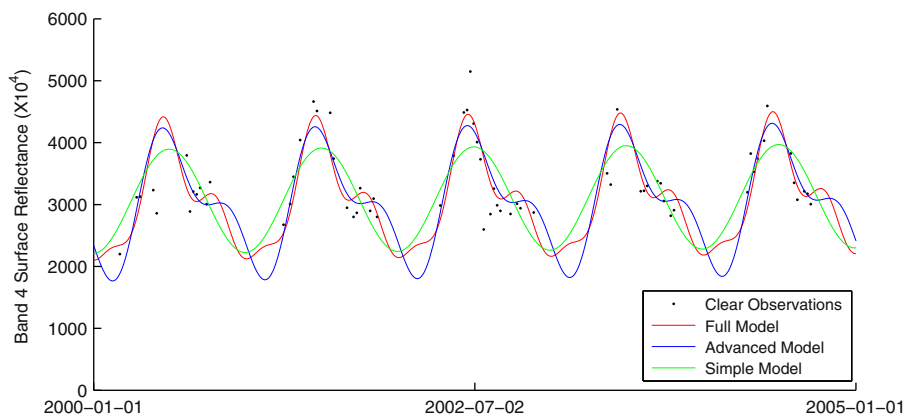


Fig. 2. Time series models estimated for Band 4 surface reflectance using all available Landsat observations between 2001 and 2004 for a crop pixel. The black points are the all available clear Landsat observations. The green line is the Band 4 surface reflectance estimated by the simple model. The blue line is the Band 4 surface reflectance estimated by the advanced model. The red line is the Band 4 surface reflectance estimated by the full model. Note that the more complex the time series model is, the better the performance in modeling the intra-annual differences in the time series data. (For interpretation of the references to color in this figure legend, the reader is referred to the web version of this article.)

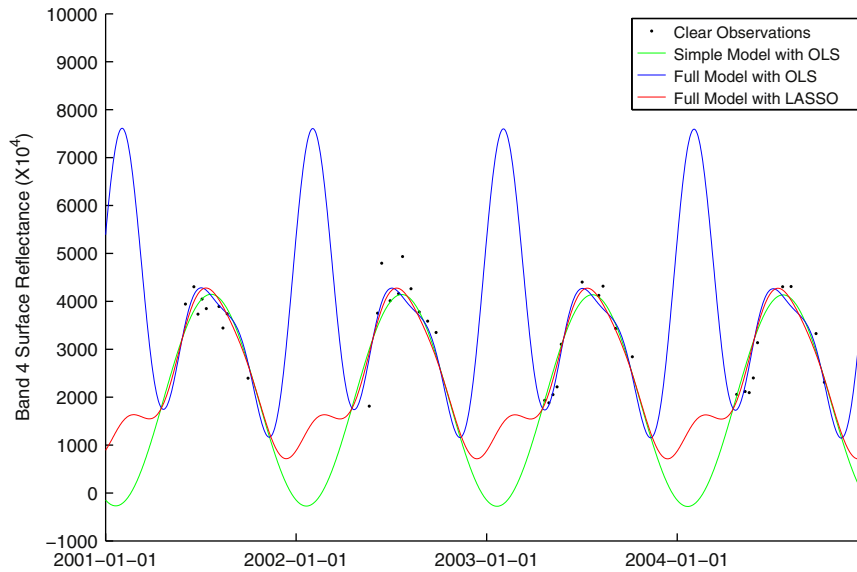


Fig. 3. Time series model estimated for Band 4 surface reflectance using all available Landsat observations between 2001 and 2004 for a deciduous forest. The black points are the all available clear Landsat observations. The green line is the Band 4 surface reflectance estimated by the simple model based on OLS fit. The blue line is the Band 4 surface reflectance estimated by the full model based on OLS fit. The red line is the Band 4 surface reflectance estimated by the full model based on LASSO fit. Note that during winter time there is no clear observation due to the presence of snow. As there is no control point during winter time, both the simple and the full models tend to overfit during this time period, especially the full model, while the LASSO fit does not have this artifact even for the full model. (For interpretation of the references to color in this figure legend, the reader is referred to the web version of this article.)

a composited clear Landsat image. Moreover, the “best” observations may be selected from images acquired from different times of year and this can cause problems if there are phenology effects.

To overcome the temporal limitation of Landsat data, one solution is to “blend” Landsat images with coarse-resolution images that have much higher temporal frequency. MODIS images are the best option, as they have much higher temporal frequency (daily observations for most of the world) and very similar spectral bands (Justice et al., 2002). With the extra temporal information provided by the MODIS time series and the finer spatial resolution provided by a few Landsat

images, it is possible to predict clear daily Landsat images (Gao, Masek, Schwaller, & Hall, 2006; Hilker, Wulder, Coops, Seitz, et al., 2009; Roy et al., 2008). These “blending” algorithms are capable of providing exciting results, but also have limitations. The first limitation is that these algorithms are highly dependent on the MODIS observations which are not available prior to 2000 (Justice et al., 2002). For Landsat images acquired before 2000, it is impossible to apply this kind of method. The second limitation is that they still need a few clear Landsat images as their input, which for some places with lots of clouds may take a few years (Zhu, Woodcock, & Olofsson, 2012). The third

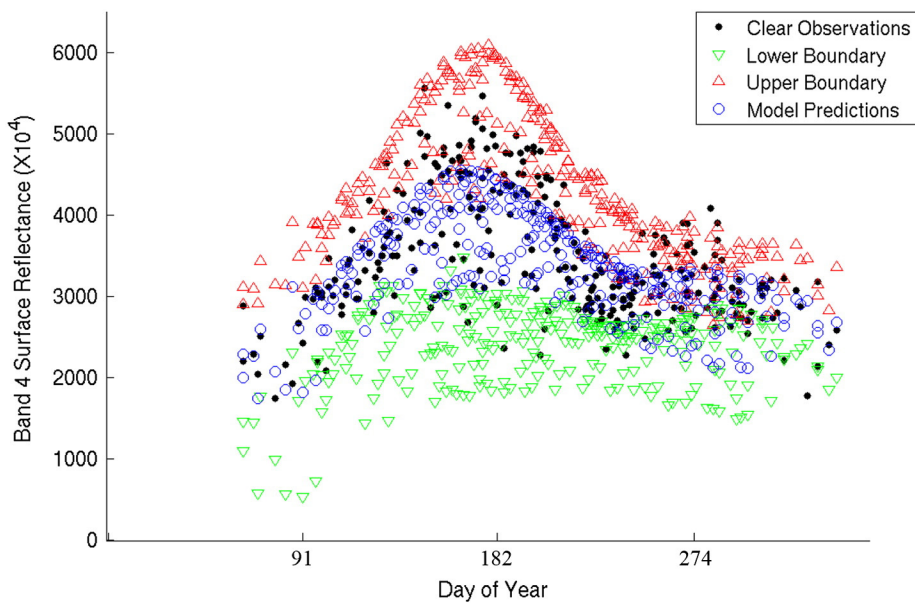


Fig. 4. This graph illustrates the temporally-adjusted RMSE used as the threshold for detecting abrupt surface change. The black points are the all available clear observations of Band 4 surface reflectance acquired on different days of the year. The blue circles are model predicted Band 4 surface reflectance generated at the same time as the real clear Landsat observations. The red upward-pointing triangles are the upper boundary of the threshold, which is the result of the model predicted Band 4 surface reflectance plus two times the temporally-adjusted RMSE. The green downward-pointing triangles are the lower boundary of the threshold that is the result of the model predicted Band 4 surface reflectance minus two times of the temporally-adjusted RMSE. Note that the variation in the data is significantly larger in growing season (middle of the year) than in the other time periods. (For interpretation of the references to color in this figure legend, the reader is referred to the web version of this article.)

Table 3
Explanations for different QA values generated for synthetic data.

QA values	Unit	Explanations
Tens	Unit	
	0	Number of clear observations ≥ 12
	1	$6 \leq$ number of clear observations < 12
	2	Number of clear observations < 6
	3	Permanent snow pixel
0		Synthetic data generated within the time range of the time series model
1		Synthetic data generated by projecting the next time series model backward in time
2		Synthetic data generated by projecting the previous time series model forward in time

limitation is that due to the big differences in spatial resolution between Landsat and MODIS, the performance of this methodology is highly depending on the patch size of the landscape and degrades when used on heterogeneous fine-grained landscapes (Gao et al., 2006; Roy et al., 2008). Finally, this kind of methodology is reported to be less effective for places where land cover change has occurred (Hilker, Wulder, Coops, Seitz, et al., 2009). While recent studies report alleviating the problems of blending Landsat and MODIS for heterogeneous areas

(Zhu, Chen, Gao, Chen, & Masek, 2010) or for places of land cover change (Hilker, Wulder, Coops, Linke, et al., 2009), the other limitations still exist.

In this paper, we propose a new algorithm that is capable of generating “synthetic” Landsat images using all available Landsat Thematic Mapper (TM) and ETM+ images. Based on time series models generated for each pixel using all available Landsat observations, synthetic Landsat images that are free of cloud, cloud shadow, and snow (except for perennial snow) from any given time (within the Landsats 4–7 era) can be generated. The model-predicted synthetic Landsat images are produced for the optical bands (Landsat TM and ETM+ Bands 1, 2, 3, 4, 5, and 7) (Table 1) and the last band is a Quality Assessment (QA) Band. The synthetic images are designed to provide consistent Landsat data that can be used to derive land cover and bio-physical products.

2. Study area and Landsat data

2.1. Study area

The study area includes six Landsat scenes at different places in the Conterminous United States (Fig. 1). The selected Landsat scenes cover a variety of forested ecosystems across axes of sparse to dense tree canopies, broadleaf deciduous to evergreen conifer dominance,

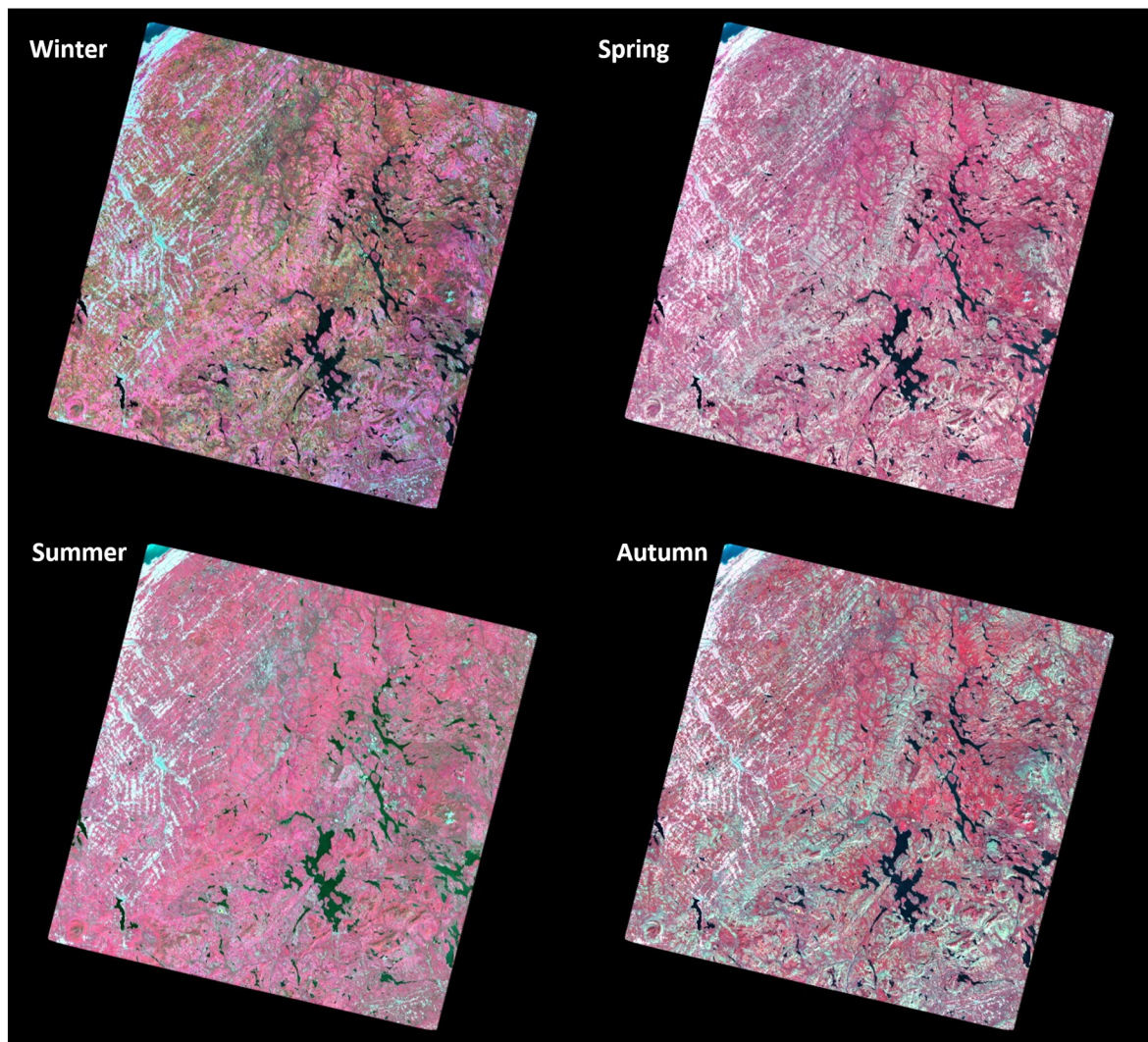


Fig. 5. Four seasonal synthetic Landsat images (Feb. 4th for winter; May 5th for spring; Aug. 6th for summer; Nov. 6th for autumn) in 2010 at 12/28 (Path/Row). Each image is a composite of synthetic Landsat Bands 4, 3, and 2.

and disturbance drivers from land use change to forest management to insect and fire.

2.2. Landsat data

All available Level 1 Terrain (corrected) (L1T) Landsat TM/ETM+ images for Worldwide Reference System (WRS) 27/27, 12/28, 45/30, 35/32, 14/32, and 16/37 (Path/Row) with more than 20% clear observations are used (Fig. 1). The percentages of clear observations are estimated based on a newly developed cloud, cloud shadow, and snow detection algorithm called Fmask (Zhu & Woodcock, 2012; Zhu, Wang, & Woodcock, 2015). Except for the thermal band, all six optical Landsat bands (Bands 1, 2, 3, 4, 5, and 7) are used as input to generate synthetic Landsat images (Table 1). The total number of available Landsat images is quite variable for different Paths/Rows (Table 2). Generally, the lower the latitude, the more Landsat images are available. This is mostly because there is less snow at lower latitudes. The two sites (27/27 and 12/28) with the least available Landsat images are located at high latitudes (Table 2). The time of the first and last images for each site are also slightly different due to the availability of the data and the time when all available Landsat data for each Landsat scene was downloaded. For all six sites, the first Landsat images are acquired between Nov. 27th, 1982 and June 26th, 1984 and the last Landsat images are acquired between July 25th, 2013 and Sept. 28th, 2013.

3. Methods

3.1. Image preprocessing

All the Landsat images are atmospherically corrected to Surface Reflectance (SR) using the Landsat Ecosystem Disturbance Adaptive Processing System (LEDAPS) algorithm (Masek et al., 2006; Vermote et al., 1997). This algorithm uses the Second Simulation of the Satellite Signal in the Solar Spectrum (6S) radiative transfer model for atmosphere correction. Next, a two-step cloud, cloud shadow, and snow screening is applied to all available observations. The first step is a single-date algorithm called Fmask that detects cloud, cloud shadow, and snow based on the spectral and context information extracted from a single Landsat image (Zhu & Woodcock, 2012; Zhu, Wang, & Woodcock, 2015). The second step is based on the results of the first step and uses the extra temporal information to further screen outliers that are previously missed in the first step (Zhu & Woodcock, 2014a; Zhu & Woodcock, 2014b).

3.2. Estimating the time series model

3.2.1. Time series models

For every pixel in the Landsat images, there is at least one time series model estimated for each spectral band, and the number of estimated

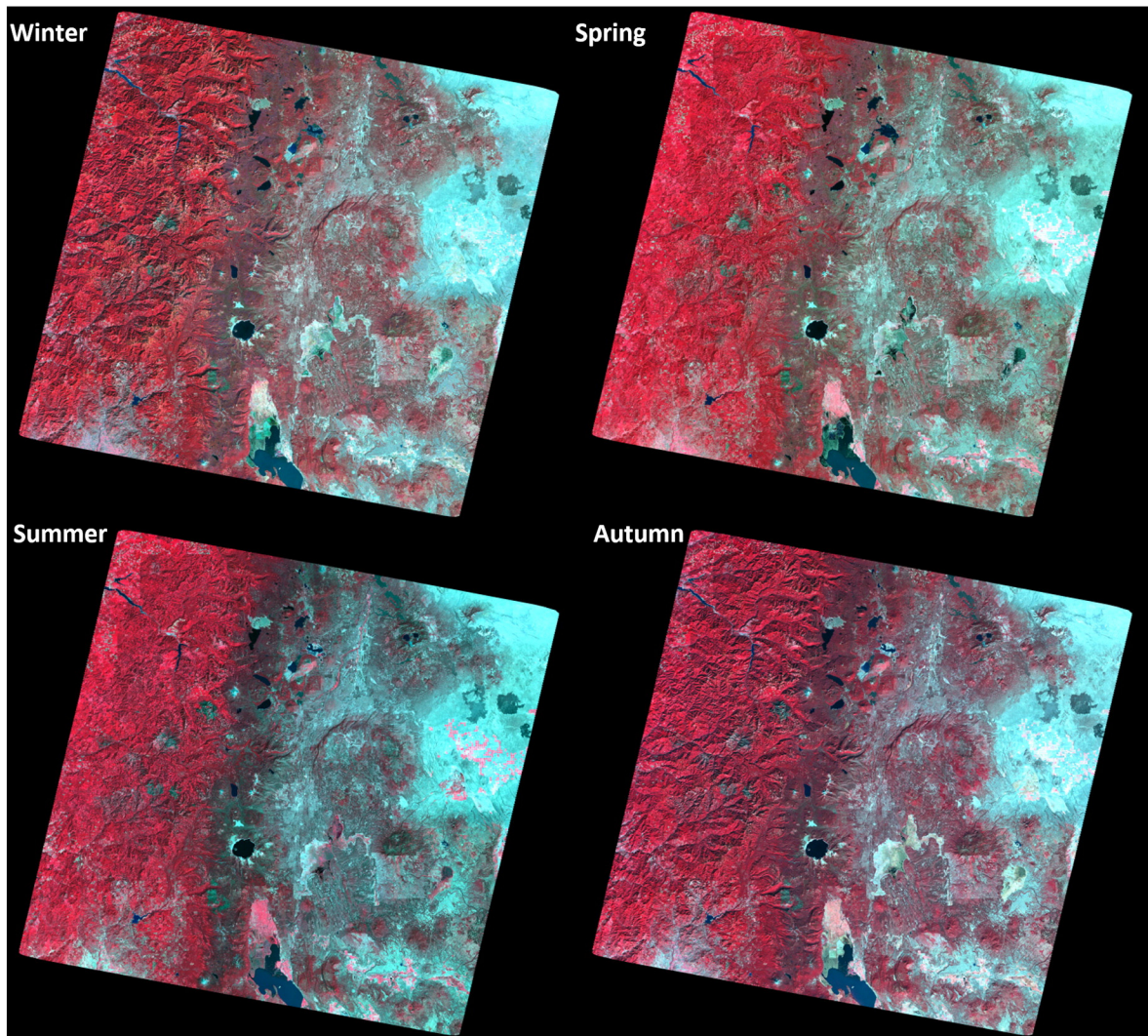


Fig. 6. Four seasonal synthetic Landsat images (Feb. 4th for winter; May 5th for spring; Aug. 6th for summer; Nov. 6th for autumn) in 2010 at 45/30 (Path/Row). Each image is a composite of synthetic Landsat Bands 4, 3, and 2.

time series model is dependent on the number of abrupt surface changes that are detected. Three different time series models, consisted of harmonic (Fourier) models (Davis, 1986; Rayner, 1971) and a long-term trend component, are used for estimating surface reflectance for different spectral bands. The first time series model (hereafter will be called “simple model”) has only four coefficients (Eq. 1) and it has been successfully applied for Continuous Change Detection and Classification (CCDC) of land cover for a Landsat scene located in New England, USA (Zhu & Woodcock, 2014b). The first coefficient ($a_{0,i}$) is used for estimating the overall value for the i th Landsat Band. The second and third coefficients ($a_{1,i}$, $b_{1,i}$) are used to model the intra-annual changes caused by phenology and sun angle differences for the i th Landsat Band. The last coefficient ($c_{1,i}$) is the only term that makes the time series models different from harmonic (Fourier) models. It is used to estimate the long-term trend for the i th Landsat Band, and this information would be very critical for capturing gradual surface changes that are more persistent over time. This simple model works well for one of the New England Landsat scenes, however, it may have problem for places where intra-annual changes do not follow this simple model. Therefore, if more clear observations are available, a more advanced model (hereafter will be called “advanced model”) consisting of six coefficients is used (Eq. 2). Compared to the simple model, the advanced model has two more coefficients ($a_{2,i}$, $b_{2,i}$) that allow for bimodal change. A similar model has been used in the Continuous Monitoring of Forest Disturbance

Algorithm (CMFDA) for one Landsat scene located between Georgia and South Carolina, USA (Zhu et al., 2012). When there are more clear observations available, a model consisting of eight coefficients (hereafter will be called “full model”) will be applied (Eq. 3). The full model has all the components of the advanced model and it has two more coefficients allowing for intra-annual trimodal change ($a_{3,i}$, $b_{3,i}$). A similar model has been used for detecting forest disturbance in near real-time using satellite image time series (Verbesselt, Zeileis, & Herold, 2012).

$$\hat{\rho}(i, x)_{\text{simple}} = a_{0,i} + a_{1,i} \cos\left(\frac{2\pi x}{T}\right) + b_{1,i} \sin\left(\frac{2\pi x}{T}\right) + c_{1,i} x \quad (1)$$

$$\{T_{k-1}^* < x \leq T_k^*\}$$

where,

x	Julian date
i	the i th Landsat Band ($i = 1, 2, 3, 4, 5,$ and 7)
T	number of days per year ($T = 365.25$)
$a_{0,i}$	coefficient for overall value for the i th Landsat Band
$a_{1,i}$, $b_{1,i}$	coefficients for intra-annual change for the i th Landsat Band
$c_{1,i}$	coefficient for inter-annual change (slope) for the i th Landsat Band
T_k^*	the k th break points

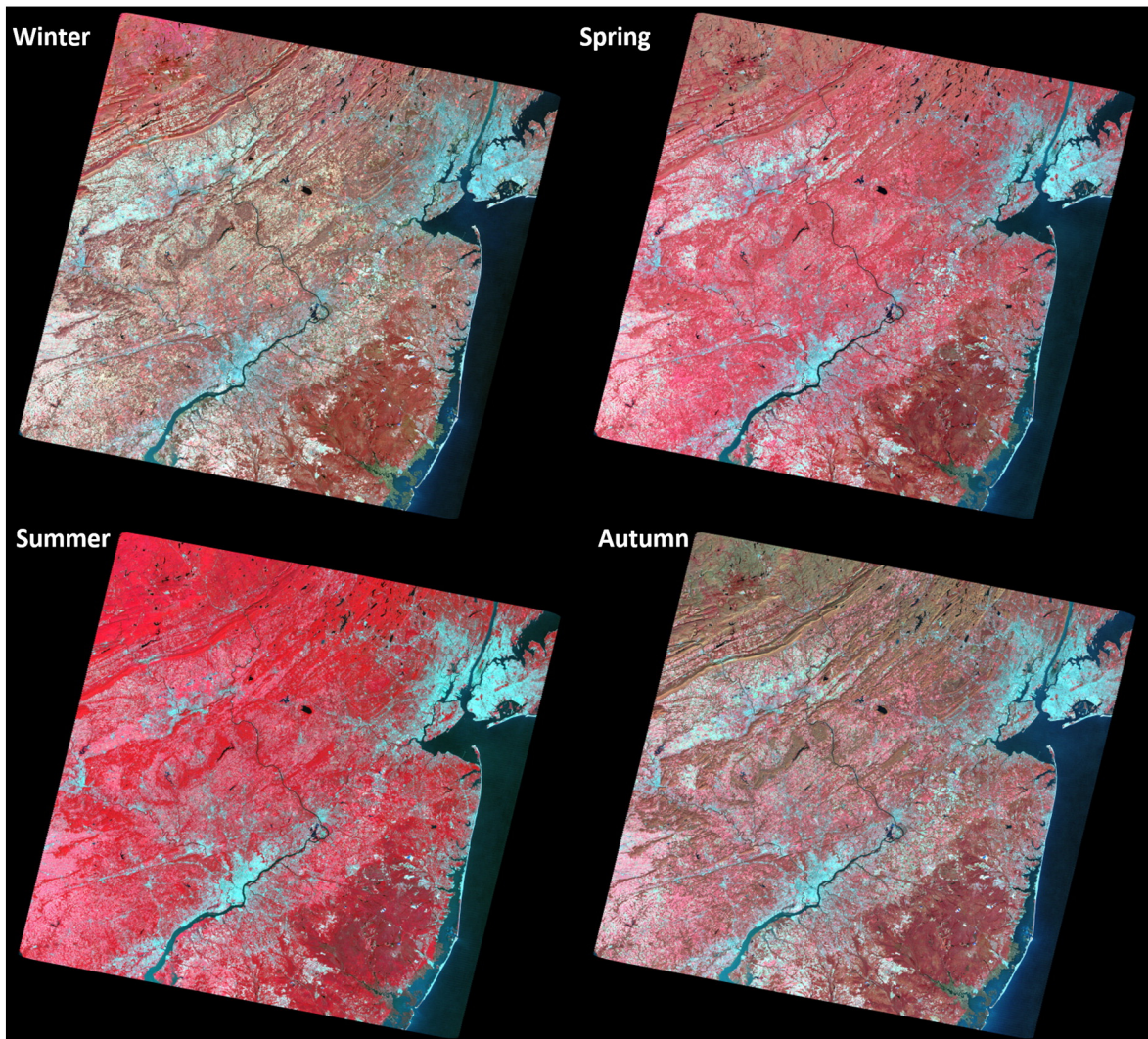


Fig. 7. Four seasonal synthetic Landsat images (Feb. 4th for winter; May 5th for spring; Aug. 6th for summer; Nov. 6th for autumn) in 2010 at 14/32 (Path/Row). Each image is a composite of synthetic Landsat Bands 4, 3, and 2.

$\hat{\rho}(i, x)_{simple}$ surface reflectance for the *i*th Landsat Band at *x* Julian date from the simple model.

$$\hat{\rho}(i, x)_{advanced} = \hat{\rho}(i, x)_{simple} + a_{2,i} \cos\left(\frac{4\pi}{T}x\right) + b_{2,i} \sin\left(\frac{4\pi}{T}x\right) \quad (2)$$

$\{\tau_{k-1}^* < x \leq \tau_k^*\}$

where,

$a_{2,i}, b_{2,i}$ coefficients for intra-annual bimodal change for the *i*th Landsat Band

$\hat{\rho}(i, x)_{advanced}$ surface reflectance for the *i*th Landsat Band at *x* Julian date from the advanced model.

$$\hat{\rho}(i, x)_{full} = \hat{\rho}(i, x)_{advanced} + a_{3,i} \cos\left(\frac{6\pi}{T}x\right) + b_{3,i} \sin\left(\frac{6\pi}{T}x\right) \quad (3)$$

$\{\tau_{k-1}^* < x \leq \tau_k^*\}$

where,

$a_{3,i}, b_{3,i}$ coefficients for intra-annual trimodal change for the *i*th Landsat Band

$\hat{\rho}(i, x)_{full}$ surface reflectance for the *i*th Landsat Band at *x* Julian date from the full model.

Fig. 2 illustrates the three different time series models estimated for Band 4 surface reflectance based on all available Landsat observations between 2001 and 2004 for a crop pixel. If the simple model (green line) is used to estimate this time series, it is not able to model the temporal trajectory of this pixel well, due to the simplicity of the model. If the advanced model (blue line) is used, it will be able to model most of the temporal variation of the data. The best result is from the full model (red line) that uses 8 coefficients to model the Band 4 surface reflectance. It is obvious that the more complex the model used, the better the performance in modeling the intra-annual differences in the time series of Landsat data.

Previous studies suggest that for model estimation to be accurate and robust, the total number of clear observations should be more than three times the number of coefficients estimated in the time series model (Zhu & Woodcock, 2014b). Therefore, if the total number of clear observations is greater than or equal to 12 but less than 18, the simple model will be used for estimating surface reflectance. Otherwise, if the total number of clear reflectance is greater than or equal to 18 but less than 24, the advanced model will be used. If the total number of clear observation is greater than or equal to 24, the full model will be applied. The time span for each time series model can be any time larger than

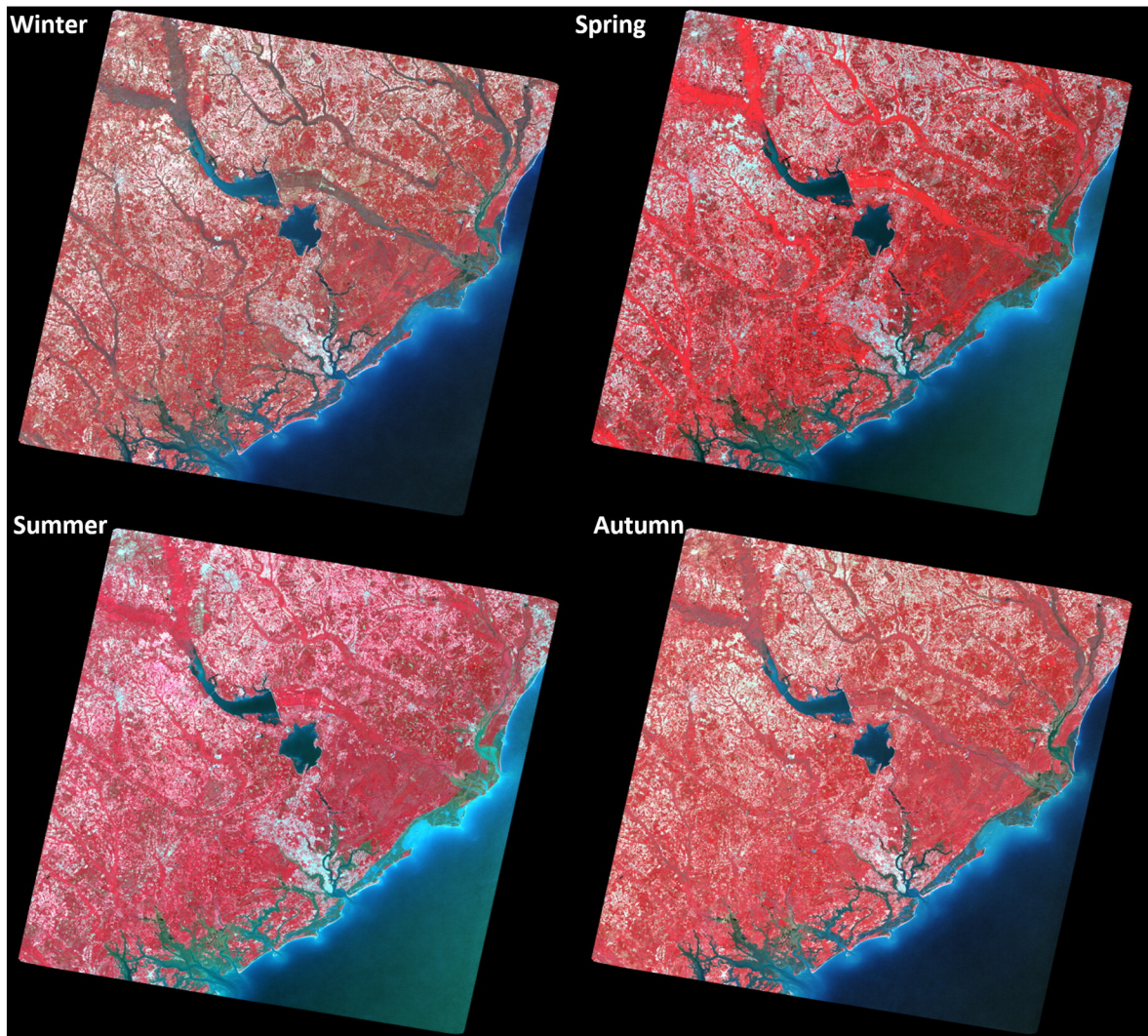


Fig. 8. Four seasonal synthetic Landsat images (Feb. 4th for winter; May 5th for spring; Aug. 6th for summer; Nov. 6th for autumn) in 2010 at 16/37 (Path/Row). Each image is a composite of synthetic Landsat Bands 4, 3, and 2.

1 year. Basically, for each pixel, the more clear observations that are available, the more complex time series model will be selected.

The additional coefficients will generally provide more accurate modeling of the temporal trajectory of the Earth's surface, but the additional coefficients can also cause problems like overfitting because of the extra freedom in the time series model, which is especially notable for the advanced and full models. Therefore, instead of using the conventional Ordinary Least Square (OLS) regression method, the Least Absolute Shrinkage and Selection Operator (LASSO) regression approach is selected for estimating all the time series models (Friedman, Hastie, Höfling, & Tibshirani, 2007; Friedman, Hastie, & Tibshirani, 2010; Hastie, Tibshirani, Friedman, & Franklin, 2005; Tibshirani, 1996). This regression method minimizes the residual sum of squared errors, with a bound on the sum of the absolute values of the coefficients (Tibshirani, 1996). In this way, some of the coefficients it produces will be exactly zero and overfitting will be greatly constrained. This special character of LASSO makes it possible to estimate time series model with more coefficients without the problem of overfitting.

Fig. 3 illustrates the three different scenarios used for estimating Band 4 surface reflectance based on all available Landsat observations between 2001 and 2005 for a deciduous forest pixel. Due to the presence of snow, there is no clear observations during the winter time, and this lack of control in this specific time period, causes both the simple model (green line) and the full model (blue line) estimation to

exhibit noticeable overfitting (false peaks or valleys), if the traditional Ordinary Least Square (OLS) fit is used. The overfitting effect is more serious for the full model with OLS fit than for the simple model with OLS fit, due to the extra freedom the full model has. However, if the LASSO fit is applied for model estimation, overfitting is reduced significantly even for the full model (red line). Therefore, by using both LASSO fit and the full model, we are able to better model the intra-annual difference in the Landsat time series and at the same time reduce the effect of overfitting.

3.2.2. Detecting abrupt surface change

If there is an abrupt surface change, this algorithm will find a break for the time series model and fit a new time series model again when there are enough newly collected clear observations. The method used for defining an abrupt surface change is similar to the approach described in the CCDC algorithm (Zhu & Woodcock, 2014b). The basic idea is to compare model predictions with real Landsat observations to find abrupt surface change. If a pixel is observed to change in multiple consecutive observations, it is identified as a change pixel.

The algorithm used here makes three major improvements in detecting abrupt surface change, compared to the CCDC algorithm. First, in the CCDC algorithm (Zhu & Woodcock, 2014b), a threshold of three times of Root Mean Square Error (RMSE) is used and three consecutive observations are required to define a change. This criterion are fine for

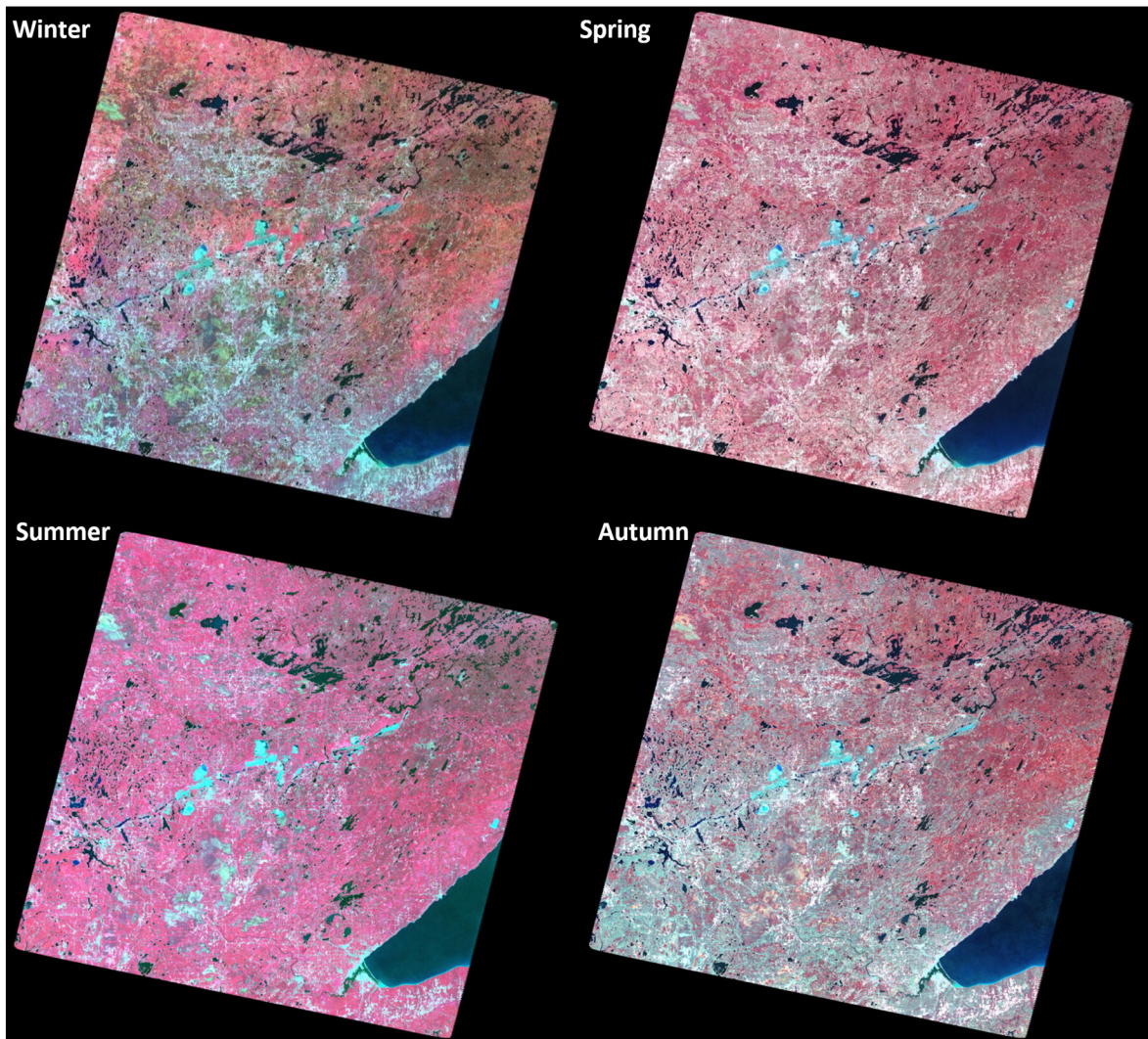


Fig. 9. Four seasonal synthetic Landsat images (Feb. 4th for winter; May 5th for spring; Aug. 6th for summer; Nov. 6th for autumn) in 2010 at 27/27 (Path/Row). Each image is a composite of synthetic Landsat Bands 4, 3, and 2.

detecting land cover change, but often misses more subtle surface changes such as burnt areas and pest-damaged forests. To capture surface changes that are more subtle, a lower threshold is used in this algorithm (two times of RMSE). However, this lower threshold will also lead to more commission errors in change detection. Therefore, this algorithm uses six consecutive observations to define an abrupt surface change, which will remove most of the false positive errors and at the same time include more subtle changes (Zhu et al., 2012). The second major improvement is that instead of using all the spectral bands for detecting surface change, this algorithm excludes the blue band and the thermal band (only using Bands 2, 3, 4, 5, and 7) in change detection. This is because these two spectral bands are quite sensitive to atmospheric influences and less sensitive to most of the surface changes. The third major improvement is that the RMSE computed for thresholding is adjusted through time in this algorithm. This is because the variation of the time series data will not be the same for different times of year. For certain times of year, the variance in the data can be much larger than the other times due to the dynamics of vegetation phenology or changes of other environment conditions. For example, there is considerable year-to-year variability in the time of green-up of forests that is related to interannual climate variability. As a result, the time series models do not fit well during the spring green-up period in some years. For our purposes, we don't want the time series models

to find minor variations in the timing of green-up as “change”. The use of a temporally-adjusted threshold essentially allows us to avoid change during periods in the year (like green-up) that are the most variable between years. Therefore, this algorithm uses the nearest (day of year) 24 observations to calculate the RMSE when the total number of clear observation is more than 24 (after the full model is used for estimating surface reflectance).

Fig. 4 illustrates how this temporally-adjusted RMSE can be used as the threshold for a crop pixel using all available Landsat observations. As the temporally-adjusted RMSE is computed based on day of year, we use the day of year as the x axis. The black points are the all available clear Landsat observations of Band 4 surface reflectance. The blue circles are model predicted Band 4 surface reflectance generated at the same time as the real clear Landsat observations. The red upward-pointing triangles are the upper boundary of the threshold, which is the result of the model predicted Band 4 surface reflectance plus two times of the temporally-adjusted RMSE. The green downward-pointing triangles are the lower boundary of the threshold, which is the result of the model predicted Band 4 surface reflectance minus two times of temporally-adjusted RMSE. Note that by using this temporally-adjusted RMSE, it is possible to generate a predicted range of thresholds that are spatially and temporally unique. For this crop pixel, it shows high variance in the summer (especially day of year near 182) and

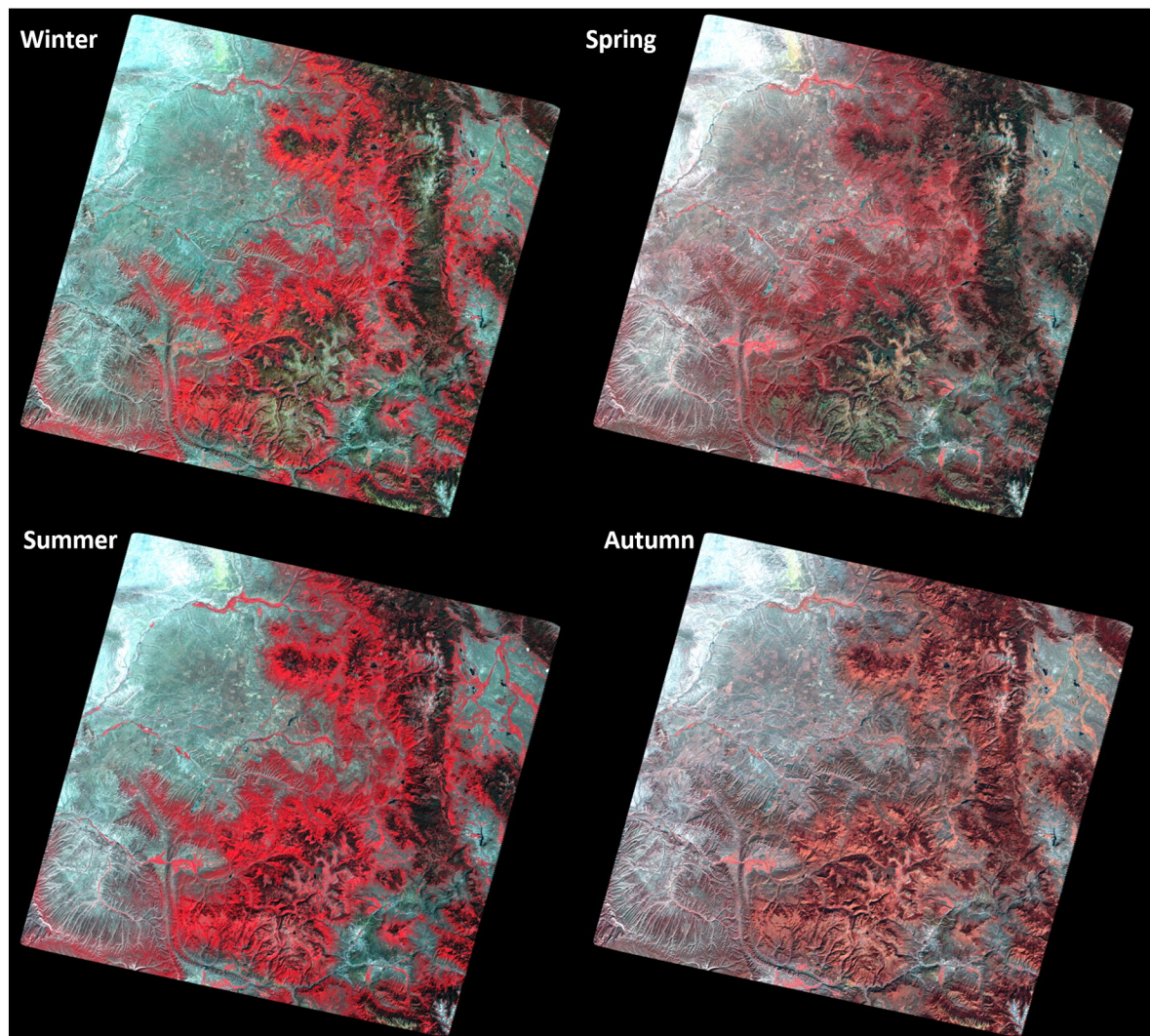


Fig. 10. Four seasonal synthetic Landsat images (Feb. 4th for winter; May 5th for spring; Aug. 6th for summer; Nov. 6th for autumn) in 2010 at 35/32 (Path/Row). Each image is a composite of synthetic Landsat Bands 4, 3, and 2.

less variability in the winter. This temporally-adjusted RMSE makes it possible to apply a larger threshold in the summer time and a smaller threshold during the winter time for change detection.

3.2.3. Backup algorithms

For most of the pixels, they will have their time series models estimated, except for pixels with less than 12 clear observations or pixels that are covered by perennial snow. To provide values for these pixels, we use backup algorithms to estimate time series model for them. For pixels with less than 12 clear observations, we treat them differently based on the total number of clear observations they have. If the total number of clear observation is more than or equal to 6, the simple model (Eq. 1) is used to estimate surface reflectance. If the total number of clear observation is less than 6 (between 1 and 5), we will use the median value of all clear observations to represent the overall surface reflectance (assumes no seasonality). For pixels that are covered by perennial snow, it is impossible to estimate time series model for clear observations, but we can still estimate snow covered surface based on all available snow observations using the simple model (Eq. 1). As

snow pixels tend to saturate in Landsat data (Dozier, 1984; Dozier, 1989), we will use all unsaturated snow observations to estimate snow covered surface reflectance. If the total number of unsaturated snow observations is less than 12, a value of 1 will be used as the surface reflectance for perennial snow pixels, as there are not enough unsaturated observations for model estimation. Note that the time series models estimated for pixels with less than 12 clear observations or covered by perennial snow are only used for generating synthetic Landsat images and they are not used for detecting surface change due to the lack of robust model estimation.

3.3. Generating synthetic Landsat images

By generating a time series model for each Landsat pixel, it is possible to predict “synthetic” Landsat images for any given day. In this paper, we evaluated this algorithm for six Landsat scenes (Fig. 1). By integrating the time variable (x : Julian date) into the estimated time series model, we are able to calculate the model predicted surface reflectance for each pixel for each spectral band. If we do this for all pixels, we are

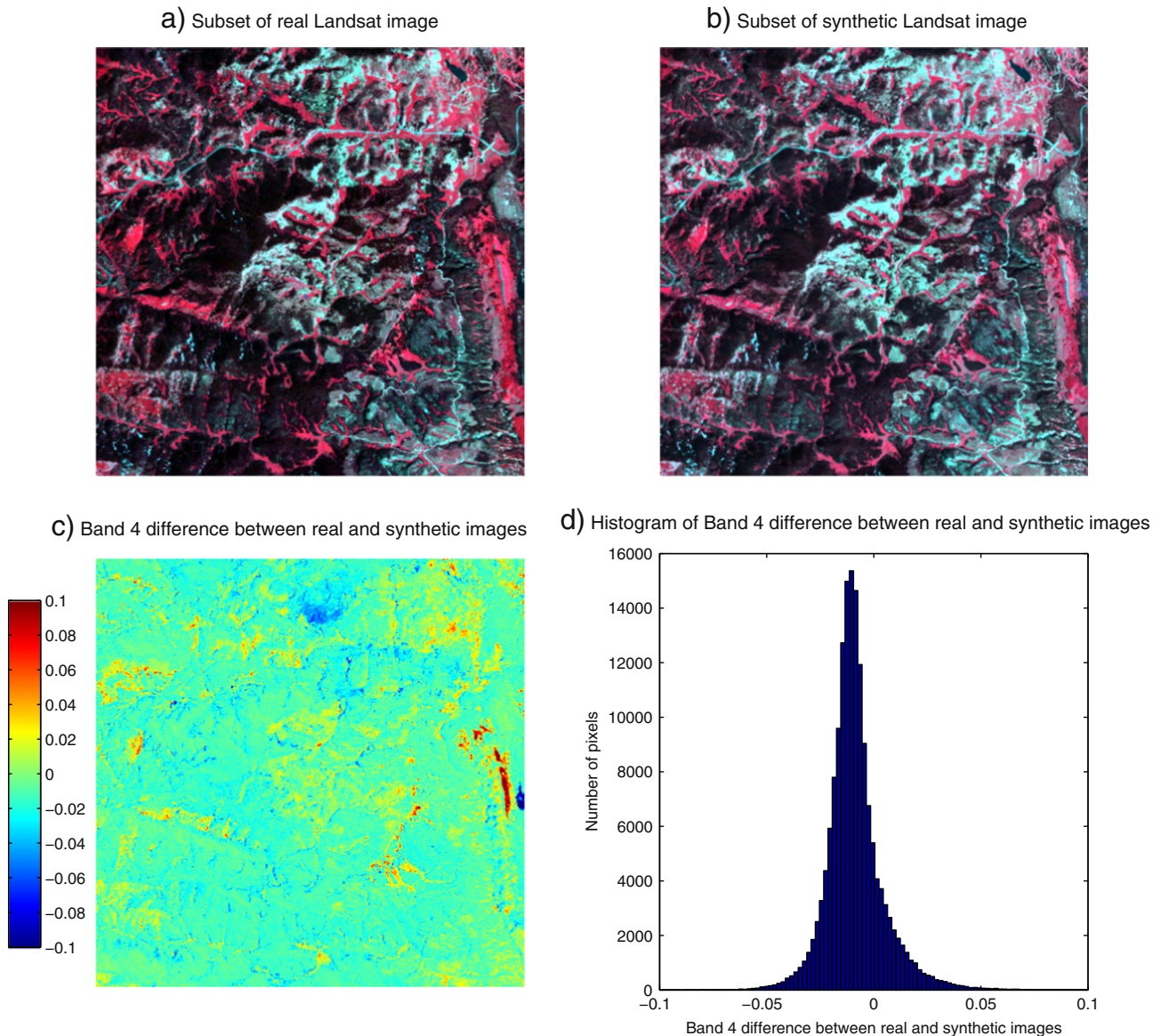


Fig. 11. a) Subset of the false color composite (Bands 4, 3, and 2) real Landsat image acquired on Aug. 6th, 1995 from Landsat scene located at 35/32 (Path/Row); b) subset of the false color composite (Bands 4, 3, and 2) synthetic Landsat image generated on Aug. 6th, 1995 for the same location; c) Band 4 difference between real and synthetic images; and d) histogram of Band 4 difference between real and synthetic images. Note that the primary forest and the wetland are very similar between the real and synthetic Landsat images. (For interpretation of the references to color in this figure legend, the reader is referred to the web version of this article.)

able to generate synthetic Landsat images for any specified date. This approach will work for most pixels most of the time, however, between the time series models estimated before and after a land surface change, there is often a time period during which the data fluctuate too much and it is impossible to initialize a time series model. For example, in many instances of land use change, there is often a disturbance at one time and then considerable fluctuation in the reflectance of the site following disturbance. One can imagine a forest area being converted to residential housing, a process common in New England. In this case, there is typically an initial disturbance (harvesting of the trees), followed by a whole series of steps necessary to prepare the site for building. Then, once home construction begins, surface reflectance will change as the work proceeds, including the time when the yards are planted and begin to take form. All these steps lead to changes in reflectance that do not vary in any organized or seasonal manner. Therefore, some pixels may have a time period when there is no time series model available. For these pixels we first check if there is a time series model estimated later in time. If there is, we project this time series model backward in time to estimate surface reflectance for times after the

last disturbance. This approach is based on the assumption that when abrupt surface change occurred, the surface reflectance is best estimated by the time series model from after the change. This assumption may ignore some kinds of land cover change that are more ephemeral, but there is really no better alternative in these cases. On the other hand, if the desired time of the synthetic images is after the end of the last time series model, we will project the last time series model forward in time to predict future surface reflectance. This approach is based on the assumption that if there is no abrupt surface change, the future surface reflectance will follow the last estimated time series model.

In addition to the model-predicted surface reflectance for the six Landsat optical bands (Table 1), a Quality Assessment (QA) Band is produced. The unit digit of the QA Band indicates how the time series model is estimated and the tens digit of the QA Band indicates how the time series model is used for generating the synthetic data (Table 3). For the unit digit in the QA Band, it can be any value between 0 and 3, and the smaller the number, the better the quality of the estimated time series model. If the unit digit is equal to 0, it means that there are more than 12 clear observations available and this time series model is

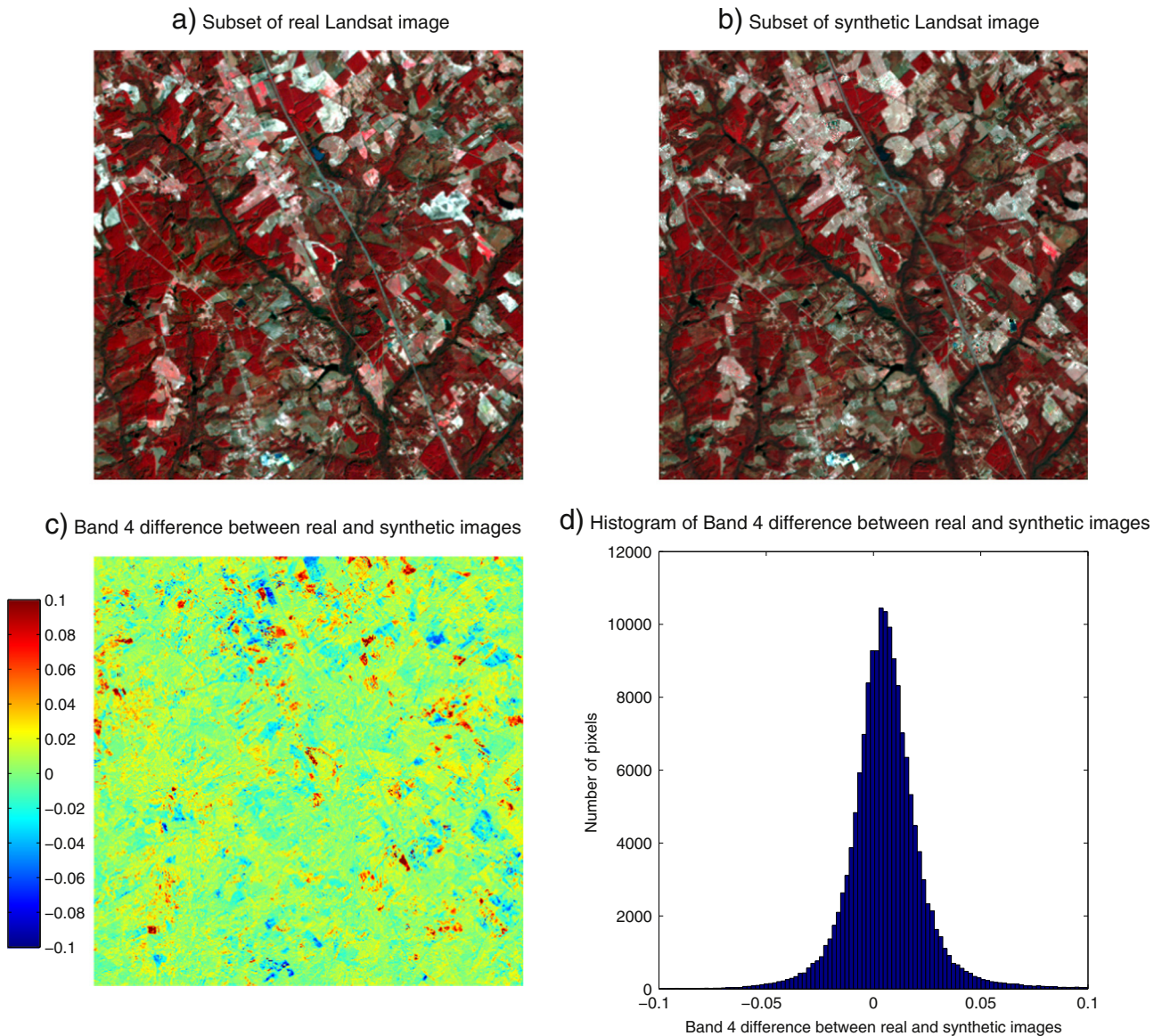


Fig. 12. a) Subset of the false color composite (Bands 4, 3, and 2) real Landsat image acquired on Feb. 4th, 2000 from Landsat scene located at 16/37 (Path/Row); b) subset of the false color composite (Bands 4, 3, and 2) synthetic Landsat image generated on Feb. 4th, 2000 for the same location; c) Band 4 difference between real and synthetic images; and d) histogram of Band 4 difference between real and synthetic images. Note that the cultivated forest and bare soil are very similar between the real and synthetic Landsat images. (For interpretation of the references to color in this figure legend, the reader is referred to the web version of this article.)

robust enough for detecting abrupt surface change. If the unit digit is equal to 1, it means that the total number of clear observations is less than 12 but more than or equal to 6 and the simple model is used to estimate surface reflectance. If the unit digit is equal to 2, it means that the total number of clear observations is less than 6 and the median value is used to represent the overall value of surface reflectance. If the unit digit is equal to 3, it means that this is a perennial snow pixel and time series model is estimated based on all available snow observations. For the tens digit in the QA Band, it can be any value between 0 and 2, and the smaller the number, the better the quality in generating the synthetic data. If the tens digit is equal to 0, it indicates that this synthetic data is generated within the time range of the time series model. If the tens digit is equal to 1, it indicates that this synthetic data is outside the time range of any time series model and it is generated by projecting the next time series model backward in time. If the tens digit is equal to 2, it indicates that this synthetic data is also outside the time range of any time series model and it is generated by projecting the previous time series model forward in time. By using the two digits of the QA Band, it is possible to know the quality of the synthetic data. For

example, if the QA value is 10, it means that this synthetic data is generated by projecting the time series model backward in time and the time series model is estimated based on time series model with more than 12 clear observations. Generally, the smaller the QA value, the better the quality of the synthetic data.

4. Results

4.1. Results of the synthetic Landsat images

To demonstrate the capability of this algorithm, we generated four seasonal (Feb. 4th for winter; May 5th for spring; Aug. 6th for summer; Nov. 6th for autumn) synthetic Landsat images between 1984 and 2012 for all six Landsat scenes. Therefore, for each Path/Row, there are a total of 116 synthetic Landsat images. In this paper, we will show the four seasonal synthetic Landsat images in one of these years (2010) for each Path/Row (Figs. 5–10). Each image is a composite of synthetic Landsat Bands 4, 3, and 2 surface reflectance. There is no cloud, cloud shadow, or snow (unless perennial snow) in the synthetic images and

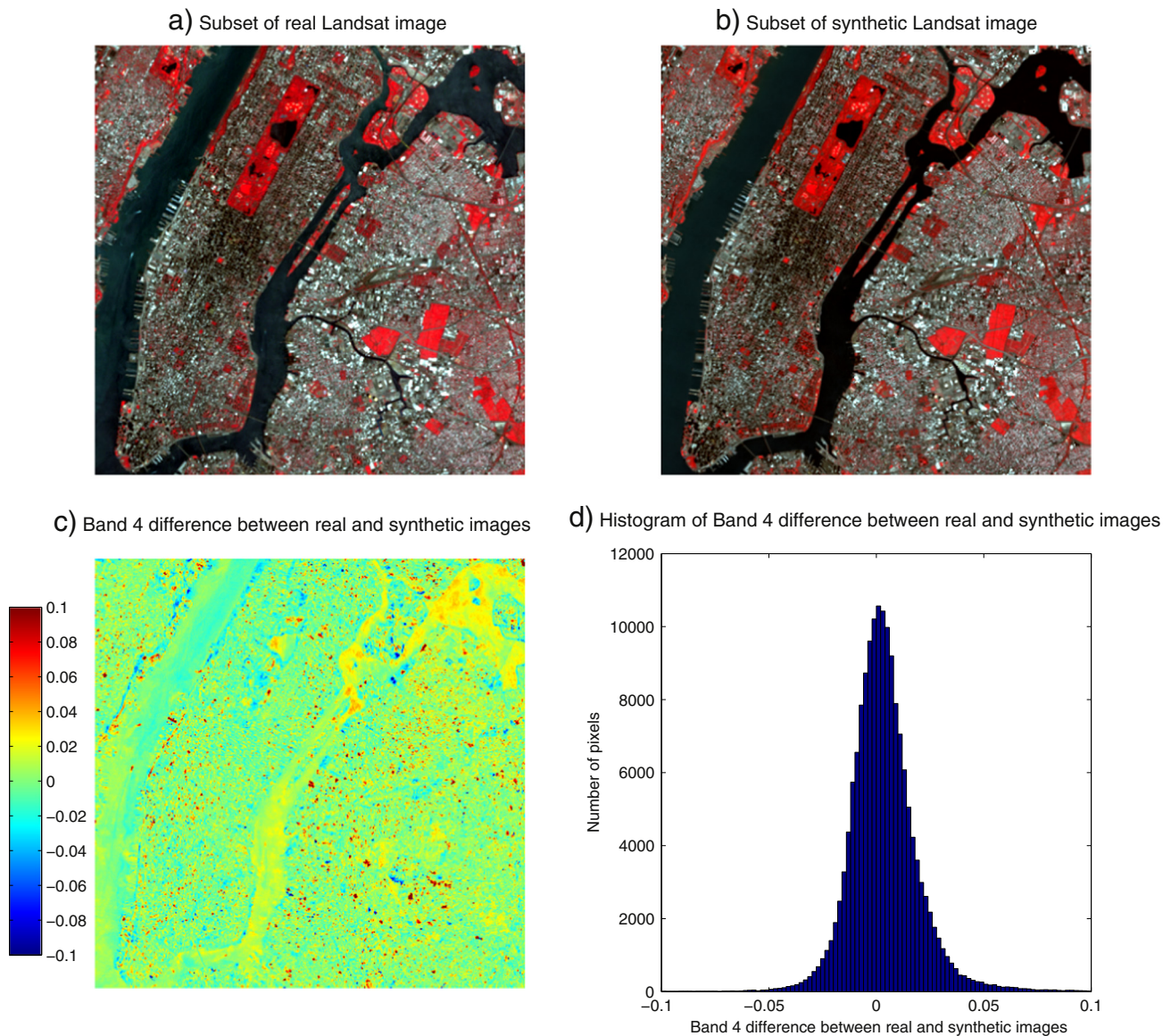


Fig. 13. a) Subset of the false color composite (Bands 4, 3, and 2) real Landsat image acquired on May 4th, 2000 from Landsat scene located at 14/32 (Path/Row); b) subset of the false color composite (Bands 4, 3, and 2) synthetic Landsat image generated on May 5th, 2000 for the same location; c) Band 4 difference between real and synthetic images; and d) histogram of Band 4 difference between real and synthetic images. Note that the urban areas and the vegetation are very similar between the real and synthetic Landsat images. (For interpretation of the references to color in this figure legend, the reader is referred to the web version of this article.)

we can easily observe the phenology differences for different kinds of land cover for different Landsat scenes (Figs. 5–10).

4.2. Accuracy assessment

To assess the accuracy of the synthetic Landsat images, we firstly visually compared several pairs of synthetic Landsat images and real Landsat images for a variety of land use and land cover types and then we quantitatively assessed the accuracy of the synthetic data by calculating the RMSE values for each band for each Path/Row using all available clear Landsat observations.

4.2.1. Visual comparison

The easiest way to check how accurate the synthetic images are is to compare them with real Landsat images acquired close in time. In this study, we have generated four seasonal Landsat synthetic images (Feb. 4th for winter; May 5th for spring; Aug. 6th for summer; Nov. 6th for autumn) for each year between 1984 and 2012 for all six

Landsat scenes. Therefore, in this section, we will compare the synthetic Landsat images with real Landsat images acquired close to them in time (± 2 days) to see how well this algorithm works. Subsets of real Landsat images and synthetic Landsat images that include primary forests, wetland, cultivated forests, urban, agriculture, residential, snow, smoke, topography shadows, clouds, cloud shadows, and lakes are shown in Figs. 11–16. Visual comparison indicates that the synthetic Landsat images are very similar to the real Landsat images for different land use and land cover types. The synthetic Landsat images can even predict image values for the land use types that change frequently such as agriculture (Fig. 14). Even illumination condition changes such as topographic shadows are correctly predicted in the synthetic images (Fig. 15). For places where the real Landsat images are covered by snow, smoke, cloud, and cloud shadow, or have SLC-off gaps, the synthetic images can still provide seamless clear observations (Fig. 15–16). Based on the spatial pattern of Band 4 difference between real and synthetic Landsat images and the histogram of Band 4 difference (Figs. 11–16c & d), most of the differences in Band 4 surface reflectance

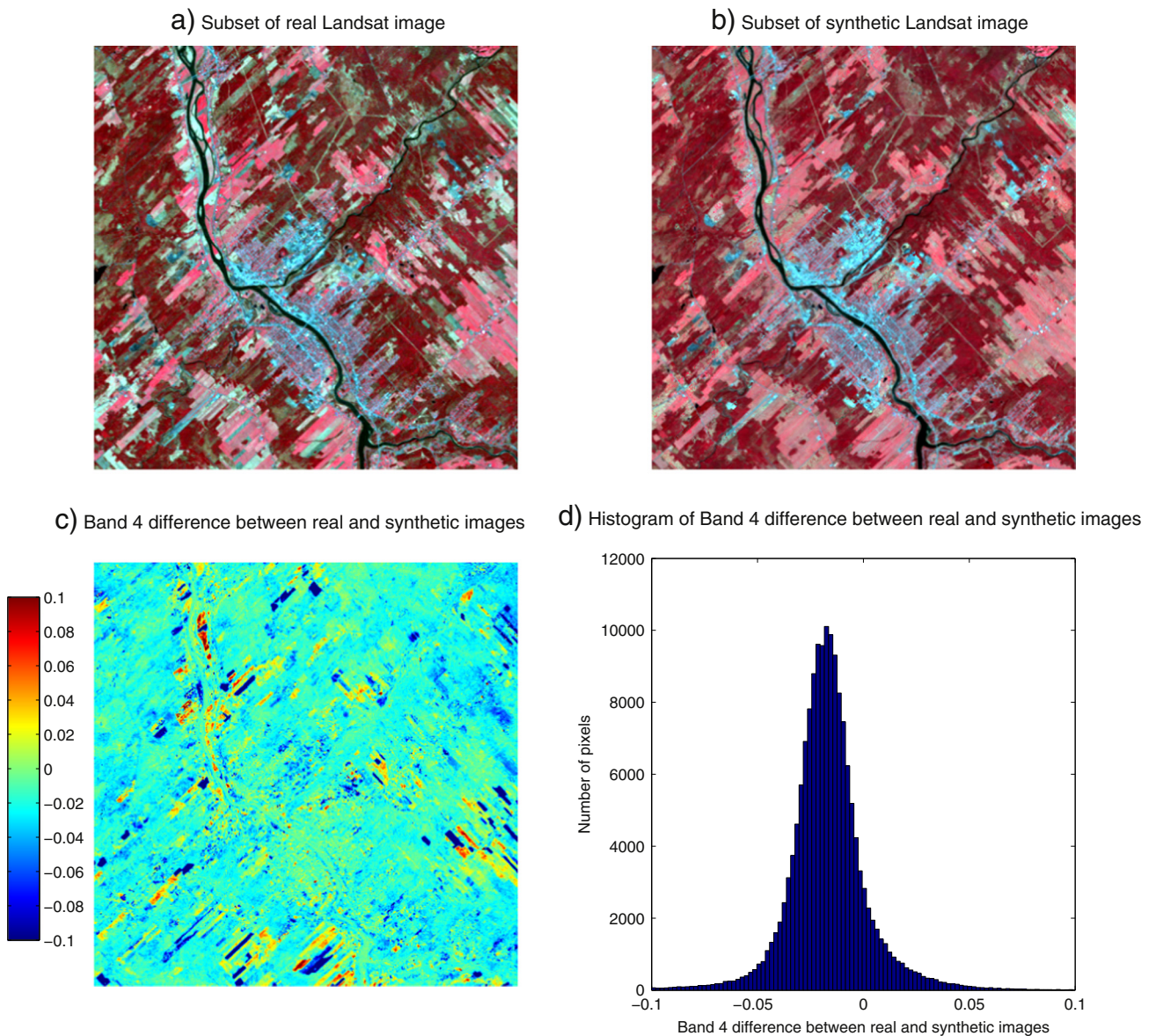


Fig. 14. a) Subset of the false color composite (Bands 4, 3, and 2) real Landsat image acquired on May 4th, 2002 from Landsat scene located at 12/28 (Path/Row); b) subset of the false color composite (Bands 4, 3, and 2) synthetic Landsat image generated on May 5th, 2002 for the same location; c) Band 4 difference between real and synthetic images; and d) histogram of Band 4 difference between real and synthetic images. Note that the low residential areas and the agriculture are very similar between the real and synthetic Landsat images. (For interpretation of the references to color in this figure legend, the reader is referred to the web version of this article.)

are less than 0.02. The predictions for agriculture and topography shadows in Band 4 are less accurate than other land surface types (Figs. 14–15c). As the synthetic images do not predict cloud, cloud shadow, and snow, these areas have large Band 4 difference (Figs. 15–16c), and this also leads to longer tails in the histogram of Band 4 difference (Figs. 15–16d).

4.2.2. Quantitative assessment

To quantitatively assess the synthetic Landsat data, we predicted the synthetic Landsat images for all available Landsat images for each site and compared them with the real Landsat images. Cloud, cloud shadow, and snow were masked out in this quantitative assessment. The RMSE between the real and synthetic images is computed for each spectral band for each site using all available clear Landsat observations (Fig. 17). The RMSE values for the visible bands (Bands 1, 2, and 3) are relatively small (approximately 0.01 in the units of surface reflectance) compare to the RMSE values for the Short-wave Infrared (SWIR) bands (between 0.01 and 0.02), and the Near Infrared (NIR) band (between 0.02 and 0.03). Due to large phenology differences, the RMSE values

for the NIR band are significantly larger than the other spectral bands. For the two Landsat scenes with less vegetation (35/32 and 45/30), the magnitude of RMSE values for the NIR bands is much smaller (~ 0.02). To help put these values in perspective, a change of 0.01 in surface reflectance corresponds to an approximately 2 DN change in the original 8-bit Landsat images. Since the RMSE values for most of the bands are around 0.01, if we convert the surface reflectance image back to DN, the difference for most of the predicted values will be around 2 DN, which is similar in magnitude (1–2 DN) to the noise levels in Landsat images (Masek, Honzak, Goward, Liu, & Pak, 2001).

5. Discussion and conclusions

The approach presented here has many advantages. First, by using all the available Landsat observations and time series analysis, the predicted synthetic images do not have clouds, cloud shadows, snow, or Landsat 7 SLC-off gaps. Second, as the time series models are capable of modeling the seasonality of the data, the synthetic images will not be influenced by vegetation phenology and sun angle differences.

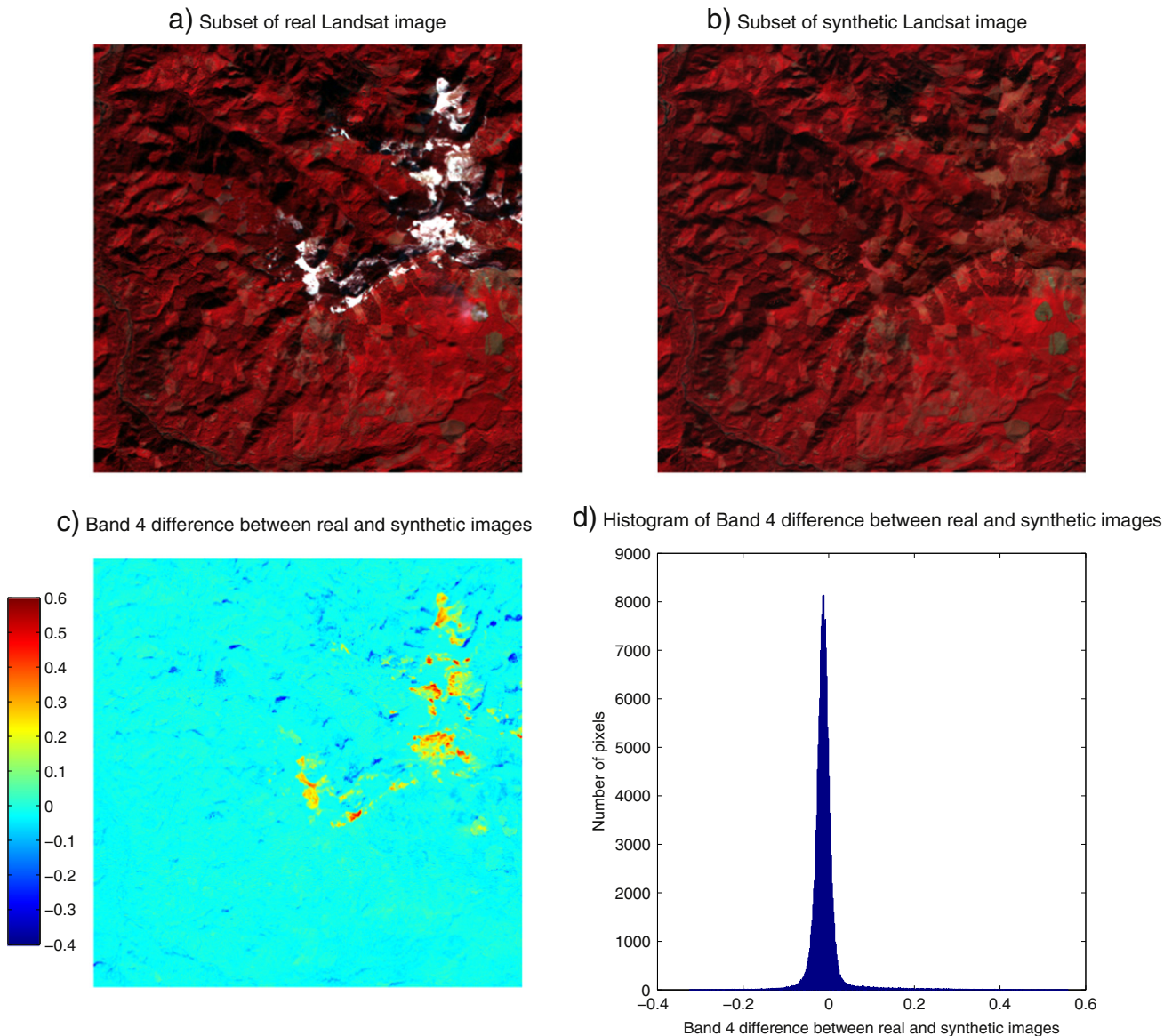


Fig. 15. a) Subset of the false color composite (Bands 4, 3, and 2) real Landsat image acquired on Nov. 8th, 2004 from Landsat scene located at 45/30 (Path/Row); b) subset of the false color composite (Bands 4, 3, and 2) synthetic Landsat image generated on Nov. 6th, 2004 for the same location; c) Band 4 difference between real and synthetic images; and d) histogram of Band 4 difference between real and synthetic images. Note that most of the topographic shadows are correctly predicted in the synthetic Landsat image and the snow and smoke that appeared in the real Landsat image do not exist in the synthetic image. (For interpretation of the references to color in this figure legend, the reader is referred to the web version of this article.)

Third, unlike other approaches that use MODIS time series to help generating synthetic Landsat images (Gao et al., 2006; Hilker, Wulder, Coops, Linke, et al., 2009; Hilker, Wulder, Coops, Seitz, et al., 2009; Roy et al., 2008; Zhu et al., 2010), this approach only uses Landsat data as its input. Therefore, it has the potential of generating synthetic Landsat images beginning from the first available Landsat image (as early as 1972). In this study, as we only use TM and ETM+ images, we are able to provide synthetic Landsat images as early as 1982 (when Landsat 4 is launched). Fourth, only Landsat pixels are used for generating synthetic data (without using MODIS), this algorithm can still achieve high accuracies in heterogeneous areas. Finally, as land surface changes are also taken into account in generating time series models, this method should not have problems in places of frequent land surface change.

The major issue with this approach is that it requires many clear Landsat observations for accurate time series model estimation. For places where clouds and snow are persistent, there may not have

been enough clear observations to estimate time series model for each pixel. This issue will be more serious for places outside of the United States, where observations are often less frequent. The launch of Landsat 8 will help with the problem because it is collecting data much more frequently than any of the previous Landsat satellites (Roy et al., 2014). In the near future, the two Sentinel 2A/2B satellites will further increase the temporal frequency of Landsat-like observations (Drusch et al., 2012). Though there are differences in the spectral bands and spatial resolutions between Landsat and Sentinel, with some simple resampling methods, it will be possible to combine Sentinel 2 observations with Landsat observations to generate synthetic data. If combining Landsat 7 and 8, and the two Sentinel 2 sensors, there will be around 10 observations per month, which will greatly improve the quality of model estimation and provide much better synthetic Landsat-like images. For places located at high latitude, persistent snow cover during winter time would also cause problems if we want to generate snow-free synthetic images. Though we used the LASSO regression to reduce

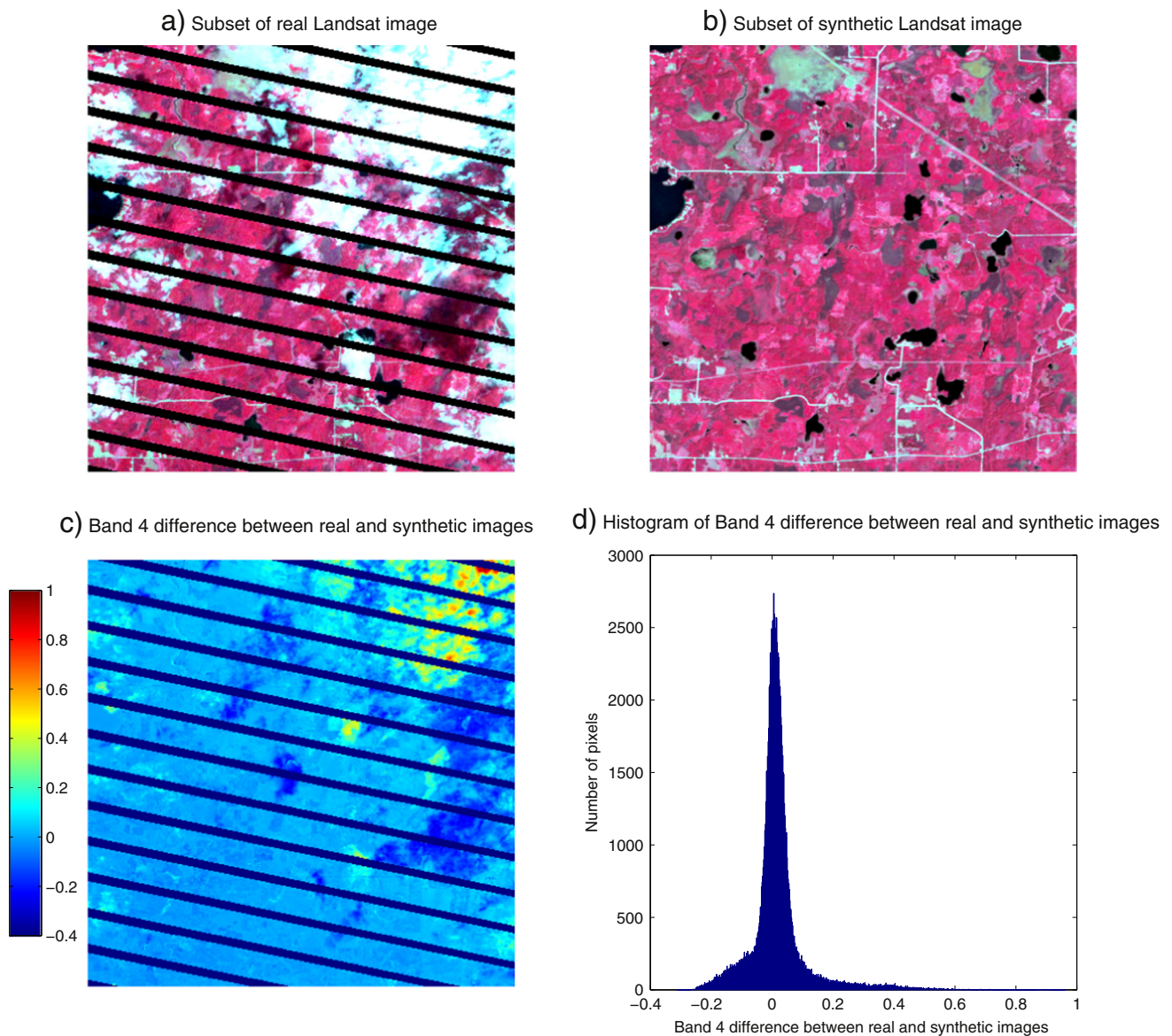


Fig. 16. a) Subset of the false color composite (Bands 4, 3, and 2) real Landsat image acquired on Aug. 4th, 2006 from Landsat scene located at 27/27 (Path/Row); b) subset of the false color composite (Bands 4, 3, and 2) synthetic Landsat image generated on Aug. 6th, 2006 for the same location; c) Band 4 difference between real and synthetic images; and d) histogram of Band 4 difference between real and synthetic images (excluding pixels located at SLC-off gaps). Note that the lakes are correctly predicted in the synthetic Landsat image and the clouds and their shadows that appeared in the real Landsat image do not exist in the synthetic image. The SLC-off gaps are filled in with predicted synthetic data. (For interpretation of the references to color in this figure legend, the reader is referred to the web version of this article.)

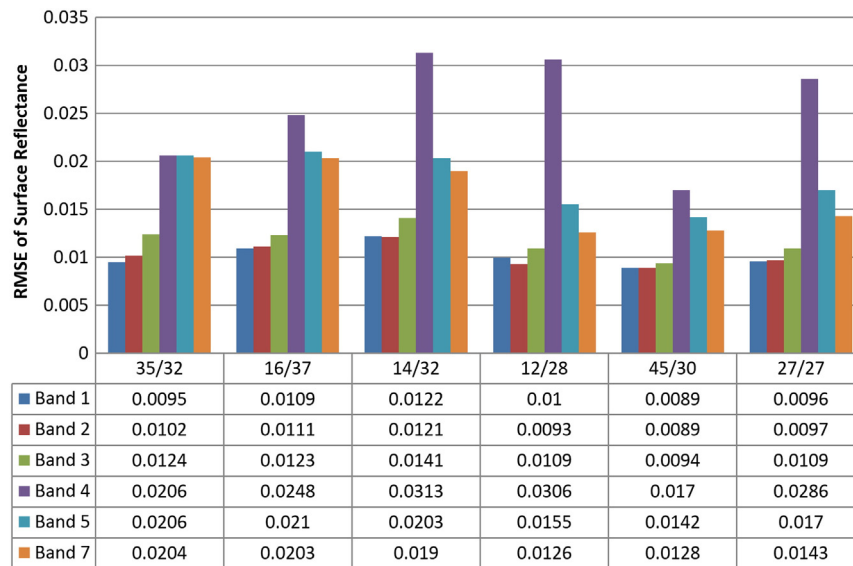


Fig. 17. Magnitude of RMSE values computed for each band and for each Path/Row. The RMSE values are calculated based on all available clear Landsat observations and the corresponding model predicted synthetic data.

overfitting during this time period, these predicted values are not always physically meaningful, as for some locations, there may not have any clear observation during the winter time.

Further work is ongoing to assess the suitability of this approach for quantitative remote sensing applications, such as deriving land cover and bio-physical products. If the synthetic Landsat data are capable of achieving good accuracies in quantitative remote sensing applications, they may be used as an alternative to real Landsat images that are usually full of gaps caused by cloud, cloud shadow, snow, and SLC-off artifacts.

Acknowledgments

We gratefully acknowledge the supports of USGS Landsat Science Team Program for Better Use of the Landsat Temporal Domain: Monitoring Land Cover Type, Condition, and Change (grant number G11PS00422), the support of NASA Earth Science U.S. Participating Investigator Program for Enhancing Compatibility of Sentinel 2 and Landsat Products for Improved Monitoring of the Earth System (grant number NNX11AE18G), and the support of USDA Forest Service Program for Testing and Developing Time Series Methods to Support Development of A Nation Landscape Change Monitoring System (grant number 13-CR-11221638-146). We would also like to extend our gratitude to the three anonymous reviewers for their thoughtful comments.

References

- Arvidson, T., Goward, S.N., Gasch, J., & Williams, D. (2006). Landsat-7 long-term acquisition plan: Development and validation. *Photogrammetric Engineering & Remote Sensing*, 72, 1137–1146.
- Cihlar, J., Manak, D., & D'orio, M. (1994). Evaluation of compositing algorithms for AVHRR data over land. *IEEE Transactions on Geoscience and Remote Sensing*, 32, 427–437.
- Davis, J.C. (1986). *Statistics and data analysis in geology* (Second Edition). New York, N.Y.: J. Wiley and Sons, 646.
- Dozier, J. (1984). Snow reflectance from Landsat-4 thematic mapper. *IEEE Transactions on Geoscience and Remote Sensing*, 3, 323–328.
- Dozier, J. (1989). Spectral signature of alpine snow cover from the Landsat Thematic Mapper. *Remote Sensing of Environment*, 28, 9–22.
- Drusch, M., Del Bello, U., Carlier, S., Colin, O., Fernandez, V., Gascon, F., et al. (2012). Sentinel-2: ESA's optical high-resolution mission for GMES operational services. *Remote Sensing of Environment*, 120, 25–36.
- Friedman, J., Hastie, T., Höfling, H., & Tibshirani, R. (2007). Pathwise coordinate optimization. *The Annals of Applied Statistics*, 1(2), 302–332.
- Friedman, J., Hastie, T., & Tibshirani, R. (2010). Regularization paths for generalized linear models via coordinate descent. *Journal of Statistical Software*, 33(1), 1–22.
- Fry, J., Xian, G., Jin, S., Dewitz, J., Homer, C., Yang, L., et al. (2011). Completion of the 2006 National Land Cover Database for the conterminous United States. *Photogrammetric Engineering and Remote Sensing*, 77(9), 858–864.
- Gao, F., Masek, J., Schwaller, M., & Hall, F. (2006). On the blending of the Landsat and MODIS surface reflectance: Predicting daily Landsat surface reflectance. *IEEE Transactions on Geoscience and Remote Sensing*, 44(8), 2207–2218.
- Griffiths, P., van der Linden, S., Kuemmerle, T., & Hostert, P. (2013). A pixel-based Landsat compositing algorithm for large area land cover mapping. *IEEE Journal of Selected Topics in Applied Earth Observations and Remote Sensing*, 6(5), 2088–2101.
- Hansen, M.C., Roy, D.P., Lindquist, E., Adusei, B., Justice, C.O., & Altstatt, A. (2008). A method for integrating MODIS and Landsat data for systematic monitoring of forest cover and change in the Congo Basin. *Remote Sensing of Environment*, 112(5), 2495–2513.
- Hastie, T., Tibshirani, R., Friedman, J., & Franklin, J. (2005). The elements of statistical learning: Data mining, inference and prediction. *The Mathematical Intelligencer*, 27(2), 83–85.
- Hermosilla, T., Wulder, M.A., White, J.C., Coops, N.C., & Hobart, G.W. (2015). An integrated Landsat time series protocol for change detection and generation of annual gap-free surface reflectance composites. *Remote Sensing of Environment*, 158, 220–234.
- Hilker, T., Wulder, M.A., Coops, N.C., Linke, J., McDermid, G., Masek, J.G., et al. (2009). A new data fusion model for high spatial- and temporal-resolution mapping of forest disturbance based on Landsat and MODIS. *Remote Sensing of Environment*, 113(8), 1613–1627.
- Hilker, T., Wulder, M.A., Coops, N.C., Seitz, N., White, J.C., Gao, F., et al. (2009). Generation of dense time series synthetic Landsat data through data blending with MODIS using a spatial and temporal adaptive reflectance fusion model. *Remote Sensing of Environment*, 113(9), 1988–1999.
- Holben, B.N. (1986). Characteristics of maximum-value composite images from temporal AVHRR data. *International Journal of Remote Sensing*, 7(11), 1417–1434.
- Ju, J., & Roy, D.P. (2008). The availability of cloud-free Landsat ETM+ data over the conterminous United States and globally. *Remote Sensing of Environment*, 112(3), 1196–1211.
- Justice, C.O., Townshend, J.R.G., Vermote, E.F., Masuoka, E., Wolfe, R.E., Saleous, N., et al. (2002). An overview of MODIS Land data processing and product status. *Remote Sensing of Environment*, 83(1), 3–15.
- Luo, Y., Trishchenko, A.P., & Khlopenkov, K.V. (2008). Developing clear-sky, cloud and cloud shadow mask for producing clear-sky composites at 250-meter spatial resolution for the seven MODIS land bands over Canada and North America. *Remote Sensing of Environment*, 112(12), 4167–4185.
- Masek, J.G., Honzak, M., Goward, S.N., Liu, P., & Pak, E. (2001). Landsat-7 ETM+ as an observatory for land cover: Initial radiometric and geometric comparisons with Landsat-5 Thematic Mapper. *Remote Sensing of Environment*, 78(1), 118–130.
- Masek, J. G., Vermote, E. F., Saleous, N., Wolfe, R., Hall, E. F., Huemmrich, F., et al. (2006). A Landsat surface reflectance data set for North America, 1990–2000. *Geoscience and Remote Sensing Letters*, 3, 68–72.
- Maxwell, S.K., Schmidt, G.L., & Storey, J.C. (2007). A multi-scale segmentation approach to filling gaps in Landsat ETM+ SLC-off images. *International Journal of Remote Sensing*, 28, 5339–5356.
- Pflugmacher, D., Cohen, W.B., & Kennedy, R.E. (2012). Using Landsat-derived disturbance history (1972–2010) to predict current forest structure. *Remote Sensing of Environment*, 122, 146–165.
- Rayner, J.N. (1971). *An introduction to spectral analysis*. London: Pion Ltd, 174.
- Roy, D.P., Ju, J., Kline, K., Scaramuzza, P.L., Kovalskyy, V., Hansen, M., et al. (2010). Web-enabled Landsat Data (WELD): Landsat ETM+ composited mosaics of the conterminous United States. *Remote Sensing of Environment*, 114(1), 35–49.

- Roy, D.P., Ju, J., Lewis, P., Schaaf, C., Gao, F., Hansen, M., et al. (2008). Multi-temporal MODIS–Landsat data fusion for relative radiometric normalization, gap filling, and prediction of Landsat data. *Remote Sensing of Environment*, 112(6), 3112–3130.
- Roy, D.P., Wulder, M.A., Loveland, T.R., Woodcock, C.E., Allen, R.G., Anderson, et al. (2014). Landsat-8: Science and product vision for terrestrial global change research. *Remote Sensing of Environment*, 145, 154–172.
- Stoms, D.M., Bueno, M.J., & Davis, F.W. (1997). Viewing geometry of AVHRR image composites derived using multiple criteria. *Photogrammetric Engineering and Remote Sensing*, 63, 681–689.
- Tibshirani, R. (1996). Regression shrinkage and selection via the lasso. *Journal of the Royal Statistical Society: Series B Methodological*, 267–288.
- Verbesselt, J., Zeileis, A., & Herold, M. (2012). Near real-time disturbance detection using satellite image time series. *Remote Sensing of Environment*, 123, 98–108.
- Vermote, E. F., El Saleous, N., Justice, C. O., Kaufman, Y. J., Privette, J. L., et al. (1997). Atmospheric correction of visible to middle-infrared EOS-MODIS data over land surfaces: Background, operational algorithm, and validation. *Journal of Geophysical Research*, 102, 17131–17141.
- White, J. C., Wulder, M. A., Hobart, G. W., Luther, J. E., Hermosilla, T., Griffiths, P., et al. (2014). Pixel-based image compositing for large-area dense time series applications and science. *Canadian Journal of Remote Sensing*, 40(3), 192–212.
- Williams, D.L., Goward, S., & Arvidson, T. (2006). Landsat: Yesterday, today, and tomorrow. *Photogrammetric Engineering and Remote Sensing*, 72, 1171–1178.
- Woodcock, C.E., Allen, R., Anderson, M., Belward, A., Bindschadler, R., Cohen, W., et al. (2008). Free access to Landsat imagery. *Science*, 320(5879), 1011.
- Wulder, M.A., Masek, J.G., Cohen, W.B., Loveland, T.R., & Woodcock, C.E. (2012). Opening the archive: How free data has enabled the science and monitoring promise of Landsat. *Remote Sensing of Environment*, 122, 2–10.
- Zhu, X., Chen, J., Gao, F., Chen, X., & Masek, J.G. (2010). An enhanced spatial and temporal adaptive reflectance fusion model for complex heterogeneous regions. *Remote Sensing of Environment*, 114(11), 2610–2623.
- Zhu, Z., Wang, S., & Woodcock, C. E. (2015). Improvement and expansion of the Fmask algorithm: cloud, cloud shadow, and snow detection for Landsats 4–7, 8, and Sentinel 2 images. *Remote Sensing of Environment*. <http://dx.doi.org/10.1016/j.rse.2014.12.014>.
- Zhu, Z., & Woodcock, C.E. (2012). Object-based cloud and cloud shadow detection in Landsat imagery. *Remote Sensing of Environment*, 118(15), 83–94.
- Zhu, Z., & Woodcock, C.E. (2014a). Automated cloud, cloud shadow, and snow detection in multitemporal Landsat data: An algorithm designed specifically for monitoring land cover change. *Remote Sensing of Environment*, 152, 217–234.
- Zhu, Z., & Woodcock, C.E. (2014b). Continuous change detection and classification of land cover using all available Landsat data. *Remote Sensing of Environment*, 144, 152–171.
- Zhu, Z., Woodcock, C.E., & Olofsson, P. (2012). Continuous monitoring of forest disturbance using all available Landsat imagery. *Remote Sensing of Environment*, 122, 75–91.